A FEM-BEM coupling scheme for elastic dynamics problems in electronic packaging

Yida He
Institute of Electronics Packaging Technology and Reliability
Department of Mechanic
Beijing University of Technology
Beijing, China
YiDHe@emails.bjut.edu.cn

Yanpeng Gong*
Institute of Electronics Packaging Technology and Reliability
Department of Mechanic
Beijing University of Technology
Beijing, China
yanpeng.gong@bjut.edu.cn

Hao Xu
Institute of Electronics Packaging Technology and Reliability
Department of Mechanic
Beijing University of Technology
Beijing, China
Xhao@emails.bjut.edu.cn

Fei Qin
Institute of Electronics Packaging Technology and Reliability
Department of Mechanic
Beijing University of Technology
Beijing, China
qfei@bjut.edu.cn

2024 25th International Conference on Electronic Packaging Technology (ICEPT) | 979-8-3503-5380-8/24/$31.00 ©2024 IEEE | DOI: 10.1109/ICEPT63120.2024.10668740

***Abstract*—In the field of electronic packaging structure reliability research, the Finite Element Method (FEM) is recognized as an effective and reliable approach for numerical simulation. Concurrently, the Boundary Element Method (BEM) is noted for its unique advantage of requiring discretization only at the boundary, which significantly reduces the degrees of freedom and potentially enhances the accuracy of analyses. This characteristic makes BEM particularly useful for analyzing multiscale structures in electronic packaging. Nevertheless, both methods have their limitations: FEM necessitates elements within the internal domain, making it computationally intensive, while BEM is most effective with linear problems and can be less versatile with nonlinear issues. Considering these factors, this paper introduces a FEM-BEM coupling algorithm designed to address the transient elastic dynamic response problem in electronic packaging structures. This approach is designed to leverage the strengths and mitigate the limitations of both the FEM and BEM. During the numerical simulation, the model is initially segmented into FE and BE domains. The FE domain is solved using ABAQUS, while the BE domain is analyzed through a self-written boundary element program. The BE domain functions as a specialized type of finite element, where its equivalent stiffness and load are determined by invoking the boundary element program via the User-Defined Element subroutine (UEL). These results are then integrated into the finite element system. Numerical examples demonstrate that the proposed FEM-BEM coupling method is both effective and feasible for analyzing the dynamic response of electronic packaging structures.**

Keywords—Electronic packaging, FEM-BEM coupling scheme, Elastic dynamics problems

I. INTRODUCTION

As electronic packaging technology progresses, electronic components may fail due to thermal and mechanical stresses as well as dynamic loads [1]. Approximately 25% of electronic component failures are attributed to dynamic stresses [2]. Dynamic loads may lead to fatigue damage and interface fracture of packaging structures, which affects the reliability of electronic packaging structures. It is of great value to predict and reduce the negative effects of dynamic loads.

Compared to experiments, numerical simulation offers the benefits of lower cost and higher repeatability, making it an effective tool for analyzing and understanding the dynamic response and behavior of complex structures. In the study of the reliability of electronic packaging, the FEM is one of the mainstream numerical methods used by researchers to study dynamics related problems. In [3], Xia et al. studied the vibration reliability of lead-free solder joints of package-on-package by using FEM. The results show that the larger the distance between the solder joints in the bottom package, the higher the reliability of the POP assembly. Mohammad et al. [4] proposed an equivalent static load to simulate the mechanical response of electronic structure under vibration load. The effectiveness of the equivalent method is verified by comparison with experiments and dynamic finite element analysis. In [5], Chandana et al. used the finite element commercial software ABAQUS to conduct dynamic drop test analysis on the ball grid array package, studied the stress in the solder joints at different positions.

For certain complex packaging structures, generating high-quality finite element meshes is challenging, which can result in decreased calculation accuracy. The BEM only needs to be discretized on the boundary of the model, which reduces the computational complexity compared with the FEM, and can be used as an effective tool to analyze the multiscale structures of electronic packaging. Khatir et al. [6] studied the thermal behavior of high power IGBT module under power cycle based on BEM, and verified the effectiveness of the numerical tool by comparing with experimental results. In [7], Yu et al. used the isogeometric boundary element method for thermal analysis of electronic packaging structures, used the radial integration method to deal with the domain integration problem caused by heat sources, and used the subregion method to deal with multi-layer structures. However, the BEM also has limitations, such as the presence of singular integrals in calculations and unsuitability for nonlinear problems.

Based on the above discussion, coupling the FEM with the BEM can solve the problem more efficiently. In general, coupling methods can be divided into two categories. The first category is to couple the BEM to the FEM, and the second category is to couple the FEM to the BEM [8]. In this paper, based on the idea of the first kind of coupling method,

the BEM will be coupled to the FEM by ABAQUS. For the proposed coupling scheme, the model is first divided into finite element and boundary element domains based on the model's geometric or material characteristics. The finite element domain is analyzed by using ABAQUS, while the boundary element domain is analyzed through a self-written transient elastic dynamics boundary element program. The boundary element domain is treated as a special type of finite element. Its equivalent stiffness matrix and load matrix are derived by running the boundary element program through the UEL subroutine. These are then integrated into the finite element system and supplied to ABAQUS to perform the finite element analysis.

II. Basic Theory of Coupling Algorithm

For structural dynamics problems, the finite element equation of the system is [9]

$$\mathbf{M}\ddot{\mathbf{u}} + \mathbf{C}\dot{\mathbf{u}} + \mathbf{K}\mathbf{u} = \mathbf{P}(t) \tag{1}$$

where $\mathbf{M}$ is the mass matrix, $\mathbf{C}$ is the damping matrix, $\mathbf{K}$ is the stiffness matrix, $\mathbf{P}$ is the nodal load matrix, $\ddot{\mathbf{u}}$, $\dot{\mathbf{u}}$ and $\mathbf{u}$ are the displacement, velocity and acceleration vectors of the system, respectively.

ABAQUS utilizes the Hilber-Hughes-Taylor implicit algorithm and the Newton-Raphson iteration method to solve Equation (1). This iterative scheme is grounded in the Newmark method, and its specific recursive relationship is expressed as follows

$$\tilde{\mathbf{K}}_{n+1}\mathbf{u}(t+\Delta t) = \tilde{\mathbf{F}}_{n+1} \tag{2}$$

$$\begin{aligned}\mathbf{u}(t+\Delta t) &= \mathbf{u}(t) + \Delta t\dot{\mathbf{u}}(t) + \left(\frac{1}{2}-\beta\right)\Delta t^2\ddot{\mathbf{u}}(t) \\ &+ \beta\Delta t^2\ddot{\mathbf{u}}(t+\Delta t)\end{aligned} \tag{3}$$

$$\dot{\mathbf{u}}(t+\Delta t) = \dot{\mathbf{u}}(t) + (1-\gamma)\Delta t\ddot{\mathbf{u}}(t) + \gamma\Delta t\ddot{\mathbf{u}}(t+\Delta t) \tag{4}$$

where the effective stiffness matrix and effective load matrix are

$$\tilde{\mathbf{K}}_{n+1} = \mathbf{K} + \frac{1}{\beta\Delta t^2}\mathbf{M} + \frac{\gamma}{\beta\Delta t}\mathbf{C} \tag{5}$$

$$\begin{aligned}\tilde{\mathbf{F}}_{n+1} &= \mathbf{P}_{n+1} + \frac{1}{\beta\Delta t^2}(\mathbf{M} + \mathbf{C}\gamma\Delta t)\left[\mathbf{u}_n + \Delta t\dot{\mathbf{u}}_n + \right. \\ &\left.\left(\frac{1}{2}-\beta\right)\Delta t^2\ddot{\mathbf{u}}_n\right] - \mathbf{C}\left[\dot{\mathbf{u}}_n + (1-\gamma)\Delta t\ddot{\mathbf{u}}_n\right]\end{aligned} \tag{6}$$

In order to control the algorithm damping, parameter α is introduced into coefficients β and γ

$$\beta = \frac{1}{4}(1-\alpha)^2, \gamma = \frac{1}{2} - \alpha \tag{7}$$

where the value of α ranges from $-1/3$ to 0.

For continuous, homogeneous and isotropic elastic bodies, in the case of small deformation, its dynamic control equation is

$$(\lambda + 2G)\nabla\nabla\cdot\mathbf{u} - G\nabla\times\nabla\times\mathbf{u} - \rho\frac{\partial^2\mathbf{u}}{\partial t^2} + \rho\mathbf{b} = 0 \tag{8}$$

where ρ is the density, $\rho\mathbf{b}$ is the body forces vector, $\mathbf{u}$ is the displacement vector, the shear modulus G and the coefficient λ satisfy the relationship

$$G = \frac{E}{2(1+\nu)}, \lambda = \frac{\nu E}{(1+\nu)(1-2\nu)} \tag{9}$$

where E is the Young's modulus and ν is Poisson's ratio.

In this paper, the analysis only considers initial displacements and velocities $\mathbf{u}_0 = \mathbf{v}_0 = 0$, and assumes there are no body forces. The boundary or internal point integral equation of the 2D elastic dynamics problem can be expressed as

$$\begin{aligned}c_{lk}^i u_k^i(\mathbf{x}^i, t) &= \int_0^{t^+}\int_\Gamma u_{lk}^*(\mathbf{x}, t-\tau; \mathbf{x}^i) p_k(\mathbf{x}, \tau) d\Gamma(\mathbf{x}) d\tau \\ &- \int_0^{t^+}\int_\Gamma p_{lk}^*(\mathbf{x}, t-\tau; \mathbf{x}^i) u_k(\mathbf{x}, \tau) d\Gamma(\mathbf{x}) d\tau\end{aligned} \tag{10}$$

where $\mathbf{x}^i$ is the ith source point and $\mathbf{x}$ is the field point. c_{lk}^i is the coefficients related to the geometric characteristics of the location of the source point, when the source point is an internal point or on the smooth boundary, the values of c_{lk}^i are δ_{lk} and $1/2\delta_{lk}$, respectively. u_k^i is the displacement of the source point i, and the fundamental solutions p_{lk}^* and u_{lk}^* of tractions and displacements can be found in [11], the subscript 'lk' represents the variable along 'k' due to the load in the 'l' direction. τ is the time when the unit pulse load is applied at the source point, and t is the time when the displacements and tractions are measured at the field points. The tractions and displacements of the field points on the boundary Γ are p_k and u_k , respectively. In addition, in order to avoid the inability to calculate the integral at the peak of the Dirac δ functions, we make $t^+ = t + \varepsilon(\varepsilon \to 0)$.

Assuming that the boundary is discretized into Ne elements, the total number of boundary nodes is N. The time domain is divided into n time steps, and the time step is Δt . Traverse the source point $\mathbf{x}^i$ through all N boundary nodes, the matrix form of the boundary integral equation can be expressed as

$$\sum_{m=1}^{n}\mathbf{H}^{nm}\mathbf{u}^m = \sum_{m=1}^{n}\mathbf{G}^{nm}\mathbf{p}^m \tag{11}$$

where at time t_m (t_m=m Δt), the displacements and tractions of all boundary nodes form $\mathbf{u}^m$ and $\mathbf{p}^m$, respectively. The fundamental solution kernel function is multiplied by the interpolation shape function and integrated over the boundary element to obtain $\mathbf{H}^{nm}$ and $\mathbf{G}^{nm}$. More details on the derivation can be found in [11].

To couple the BEM into FEM, we differentiate the node variables at the finite element domain coupling interface from the noninterface node variables based on their positions shown in Fig. 1. Then, (2) is rearranged into the following form

$$\begin{bmatrix} K_1^1 & \cdots & K_1^N & K_1^g & \cdots & K_1^l \\ \vdots & \ddots & \vdots & \vdots & \ddots & \vdots \\ K_N^1 & \cdots & K_N^N & K_N^g & \cdots & K_N^l \end{bmatrix} \times \begin{Bmatrix} u_1 \\ \vdots \\ u_N \\ u_g \\ \vdots \\ u_l \end{Bmatrix} = \begin{Bmatrix} F_1 \\ \vdots \\ F_N \\ F_g \\ \vdots \\ F_l \end{Bmatrix} \tag{12}$$

and (12) can be further written into the following matrix form

$$\begin{bmatrix} \mathbf{K}_{oo} & \mathbf{K}_{oi} \\ \mathbf{K}_{io} & \mathbf{K}_{ii} \end{bmatrix} \begin{Bmatrix} \mathbf{u}_{Fo}^{n+1} \\ \mathbf{u}_{Fi}^{n+1} \end{Bmatrix} = \begin{Bmatrix} \mathbf{F}_{Fo}^{n+1} \\ \mathbf{F}_{Fi}^{n+1} \end{Bmatrix} \tag{13}$$

where the subscript Fi represents the nodes at the coupling interface, and Fo represents the noninterface nodes. The $\mathbf{K}$ and $\mathbf{F}$ are rearranged by $\tilde{\mathbf{K}}$ and $\tilde{\mathbf{F}}$, respectively.

$$\begin{bmatrix} \mathbf{K}_{oo} & \mathbf{K}_{oi} \\ \mathbf{K}_{io} & \mathbf{K}_{ii} \end{bmatrix} = \begin{bmatrix} \tilde{\mathbf{K}}_{oo} + a_0\mathbf{M}_{oo} & \tilde{\mathbf{K}}_{oi} + a_0\mathbf{M}_{oi} \\ \tilde{\mathbf{K}}_{io} + a_0\mathbf{M}_{io} & \tilde{\mathbf{K}}_{ii} + a_0\mathbf{M}_{ii} \end{bmatrix} \tag{14}$$

$$\begin{Bmatrix} \mathbf{F}_{Fo}^{n+1} \\ \mathbf{F}_{Fi}^{n+1} \end{Bmatrix} = \begin{Bmatrix} \mathbf{P}_{Fo}^{n+1} \\ \mathbf{P}_{Fi}^{n+1} \end{Bmatrix} + \begin{bmatrix} \mathbf{M}_{oo} & \mathbf{M}_{oi} \\ \mathbf{M}_{io} & \mathbf{M}_{ii} \end{bmatrix} \begin{Bmatrix} \mathbf{f}_{Fo}^{n} \\ \mathbf{f}_{Fi}^{n} \end{Bmatrix} \tag{15}$$

In (15)

$$\begin{Bmatrix} \mathbf{f}_{Fo}^{n} \\ \mathbf{f}_{Fi}^{n} \end{Bmatrix} = \begin{Bmatrix} a_0\mathbf{u}_{Fo}^{n} + a_1\dot{\mathbf{u}}_{Fo}^{n} + a_2\ddot{\mathbf{u}}_{Fo}^{n} \\ a_0\mathbf{u}_{Fi}^{n} + a_1\dot{\mathbf{u}}_{Fi}^{n} + a_2\ddot{\mathbf{u}}_{Fi}^{n} \end{Bmatrix} \tag{16}$$

$$a_0 = \frac{1}{\beta\Delta t^2},\quad a_1 = \frac{1}{\beta\Delta t},\quad a_2 = \frac{1}{2\beta} - 1 \tag{17}$$

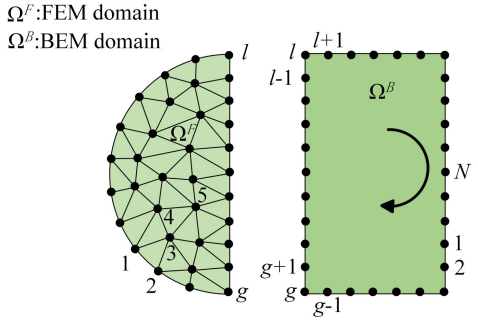

Fig. 1. Meshes and nodal locations of the two domains.

Similarly, all node variables on the coupled interface and noninterface of the boundary element domain can be reassembled, and (11) can be rewritten as

$$\begin{bmatrix} \mathbf{H}_{ii} & \mathbf{H}_{io} \\ \mathbf{H}_{oi} & \mathbf{H}_{oo} \end{bmatrix} \begin{Bmatrix} \mathbf{u}_{Bi}^{n+1} \\ \mathbf{u}_{Bo}^{n+1} \end{Bmatrix} = \begin{bmatrix} \mathbf{G}_{ii} & \mathbf{G}_{io} \\ \mathbf{G}_{oi} & \mathbf{G}_{oo} \end{bmatrix} \begin{Bmatrix} \mathbf{p}_{Bi}^{n+1} \\ \mathbf{p}_{Bo}^{n+1} \end{Bmatrix} + \begin{Bmatrix} \mathbf{r}_{Bi}^{n} \\ \mathbf{r}_{Bo}^{n} \end{Bmatrix} \tag{18}$$

$$\begin{Bmatrix} \mathbf{r}_{Bi}^{n} \\ \mathbf{r}_{Bo}^{n} \end{Bmatrix} = \sum_{\mathrm{m}=1}^{\mathrm{n}} [\mathbf{G}^{nm}\mathbf{p}^{m} - \mathbf{H}^{nm}\mathbf{u}^{m}] \tag{19}$$

where the subscript Bi represents the nodes at the coupling interface, and Bo represents the noninterface nodes.

For system of equations (18), perform partial elimination by setting $\mathbf{H}_{io} = 0$, transforming the equation into the following form

$$\begin{bmatrix} \mathbf{C}_{ii} & \mathbf{0} \\ \mathbf{C}_{oi} & \mathbf{C}_{oo} \end{bmatrix} \begin{Bmatrix} \mathbf{u}_{Bi}^{n+1} \\ \mathbf{u}_{Bo}^{n+1} \end{Bmatrix} = \begin{bmatrix} \mathbf{D}_{ii} & \mathbf{D}_{io} \\ \mathbf{D}_{oi} & \mathbf{D}_{oo} \end{bmatrix} \begin{Bmatrix} \mathbf{p}_{Bi}^{n+1} \\ \mathbf{p}_{Bo}^{n+1} \end{Bmatrix} + \begin{Bmatrix} \hat{\mathbf{r}}_{Bi}^{n} \\ \hat{\mathbf{r}}_{Bo}^{n} \end{Bmatrix} \tag{20}$$

where $\left[\hat{\mathbf{r}}_{Bi}^{n}, \hat{\mathbf{r}}_{Bo}^{n}\right]^{\mathrm{T}}$ is the result of the same elimination transformations for $\left[\mathbf{r}_{Bi}^{n}, \mathbf{r}_{Bo}^{n}\right]^{\mathrm{T}}$. Through (20), we further obtain

$$\mathbf{C}_{ii}\mathbf{u}_{Bi}^{n+1} = \mathbf{D}_{ii}\mathbf{p}_{Bi}^{n+1} + \mathbf{D}_{io}\mathbf{p}_{Bo}^{n+1} + \hat{\mathbf{r}}_{Bi}^{n} \tag{21}$$

then multiply both sides of (21) by $\mathbf{D}_{ii}^{-1}$ and rearrange the terms, we can get the expression of the tractions represented by the displacements

$$\mathbf{p}_{Bi}^{n+1} = \mathbf{D}_{ii}{}^{-1}\mathbf{C}_{ii}\mathbf{u}_{Bi}^{n+1} - \mathbf{D}_{ii}{}^{-1}\mathbf{D}_{io}\mathbf{p}_{Bo}^{n+1} - \mathbf{D}_{ii}{}^{-1}\hat{\mathbf{r}}_{Bi}^{n} \tag{22}$$

The algorithm in this paper adopts the scheme of coupling the BEM to FEM, so the nodal tractions $\mathbf{p}_{Bi}^{n+1}$ for BEM need to be converted into the equivalent nodal forces $\mathbf{F}_{Bi}^{n+1}$ used in FEM by using the following equation

$$\begin{aligned} \mathbf{F}_{Bi}^{n+1} &= \mathbf{M}_B\mathbf{p}_{Bi}^{n+1} = \mathbf{M}_B\mathbf{D}_{ii}{}^{-1}\mathbf{C}_{ii}\mathbf{u}_{Bi}^{n+1} - \mathbf{M}_B\mathbf{D}_{ii}{}^{-1} \\ \left(\mathbf{D}_{io}\mathbf{p}_{Bo}^{n+1} + \hat{\mathbf{r}}_{Bi}^{n}\right) &= \mathbf{K}_{Bi}^{n+1}\mathbf{u}_{Bi}^{n+1} - \bar{\mathbf{F}}_{Bi}^{n+1} \end{aligned} \tag{23}$$

where $\mathbf{M}_B$ is the converting matrix, $\mathbf{K}_{Bi}^{n+1}$ is the equivalent stiffness matrix of the BE domain, $\bar{\mathbf{F}}_{Bi}^{n+1}$ is the equivalent load array, (23) can also be written as

$$\begin{bmatrix} 0 & 0 \\ 0 & \mathbf{K}_{Bi}^{n+1} \end{bmatrix} \begin{Bmatrix} \mathbf{u}_{Fo}^{n+1} \\ \mathbf{u}_{Bi}^{n+1} \end{Bmatrix} = \begin{Bmatrix} 0 \\ \mathbf{F}_{Bi}^{n+1} + \bar{\mathbf{F}}_{Bi}^{n+1} \end{Bmatrix} \tag{24}$$

According to the compatibility conditions on the coupling interface

$$\begin{cases} \mathbf{u}_{Fi}^{n+1} = \mathbf{u}_{Bi}^{n+1} \\ \mathbf{P}_{Fi}^{n+1} = -\mathbf{F}_{Bi}^{n+1} \end{cases} \tag{25}$$

with the combination of equations (13), (15) and (24), the coupling equation can be obtained as

$$\begin{bmatrix} \mathbf{K}_{oo} & \mathbf{K}_{oi} \\ \mathbf{K}_{io} & \mathbf{K}_{ii} + \mathbf{K}_{Bi}^{n+1} \end{bmatrix} \begin{Bmatrix} \mathbf{u}_{Fo}^{n+1} \\ \mathbf{u}_{Fi}^{n+1} \end{Bmatrix} = \begin{Bmatrix} \mathbf{P}_{Fo}^{n+1} \\ \bar{\mathbf{F}}_{Bi}^{n+1} \end{Bmatrix} + \begin{bmatrix} \mathbf{M}_{oo} & \mathbf{M}_{oi} \\ \mathbf{M}_{io} & \mathbf{M}_{ii} \end{bmatrix} \begin{Bmatrix} \mathbf{f}_{Fo}^{n} \\ \mathbf{f}_{Fi}^{n} \end{Bmatrix} \tag{26}$$

III. Implementation of Coupling Algorithm

The UEL subroutine in the commercial finite element software ABAQUS offers users a convenient and open programming interface, allowing them to customize the element to suit specific research problems. The coupling algorithm integrates the boundary element program into ABAQUS using the UEL subroutine, treating the BE domain as a special type of finite element. Fig. 2 illustrates the overall technical route of the coupling algorithm. The implementation process is detailed as follows:

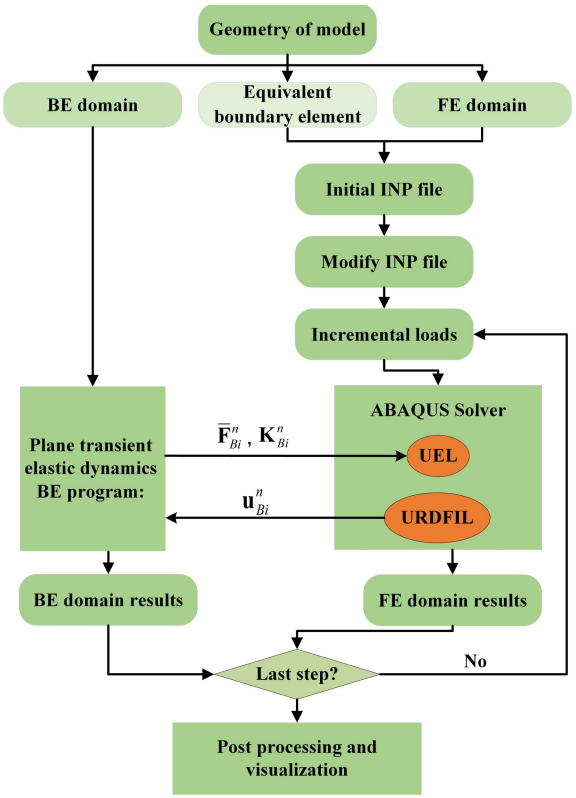

Fig. 2. The scheme of coupling algorithm

As shown in Fig. 1, based on the model's geometric or material characteristics, the numerical model is first divided into finite element and boundary element domains.

The initial coupling model is established in ABAQUS by creating a finite element domain model and an equivalent boundary element model, using the actual geometric parameters of the model. Similar to analyzing finite element problems, operations such as assigning material parameters, setting boundary conditions, and meshing are performed on both the finite element and boundary element parts. As shown in Fig. 3, in order to meet the interface compatibility conditions, The number of elements and nodes at the coupling interface are identical. The two parts are assembled together through a 'tie' connection, then output the initial INP file.

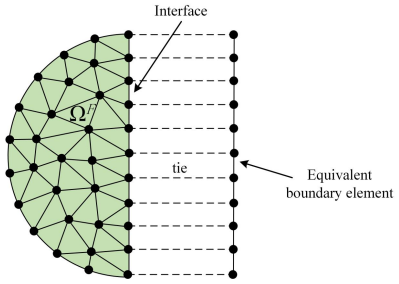

Fig. 3. Model built by ABAQUS

In the initial obtained INP file, the equivalent boundary element section only includes the geometric framework at the boundary element domain coupling interface and cannot be directly used for problem analysis. We need to modify the element properties of the equivalent boundary element section in the original INP file to *USER ELEMENT, treating the boundary element section as a 'super element'. The number of nodes in this element matches the number of nodes at the coupling interface. Then, submit the modified INP file to ABAQUS.

During numerical calculations, ABAQUS utilizes the UEL subroutine to call a self-written BEM program. This retrieves the equivalent stiffness matrix and the equivalent load array for the user-defined element, thereby achieving true coupling between the finite element domain and the boundary element domain. ABAQUS can obtain all the physical quantities within the finite element domain. Subsequently, the URDFIL subroutine is used to extract displacement values at the coupling interface, which are provided as known conditions for the boundary element program to calculate the physical quantities in the boundary element domain.

IV. Numerical Example

Using the transient response problem of a simplified package structure under dynamic load as a case study, this paper verifies the accuracy and feasibility of the coupling algorithm. Fig. 4 shows us a simplified 2D model of sintered silver structure. A SiC chip is welded to a copper substrate through a sintered silver interconnection layer. The geometric parameters of the model are given as a=1.8 mm, b=3.0 mm, c=0.5 mm, d=0.3 mm, e=0.8 mm. In the numerical model, The Young's modulus, Poisson's ratios and densities of the SiC, sintered silver and copper substrate are E_{SiC}=430000 MPa, E_{Ag}=12900 MPa, E_{Cu}=99800 MPa, ν_{SiC}=0.17, ν_{Ag}=0.1, ν_{Cu}=0.34, ρ_{SiC}=3.2 t/mm^3, ρ_{Ag}=10.49 t/mm^3, ρ_{Cu}=8.96 t/mm^3. The upper side of the SiC chip is subjected to uniform load q=1 N/mm, the load type is Heaviside loading, and the right side of model is fixed.

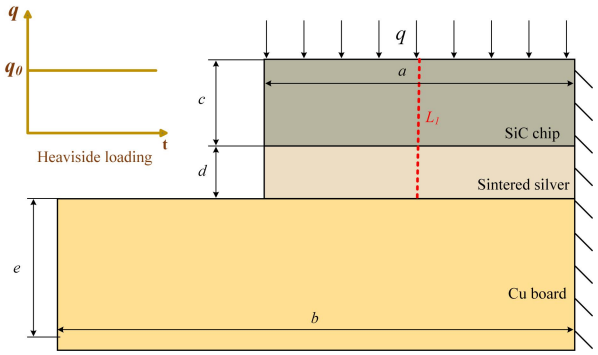

Fig. 4. Sintered silver numerical model

In the process of calculation, SiC and sintered silver are studied by FEM, while Cu substrate is analyzed by BEM. Fig. 5 shows the meshes used in the coupling algorithm.

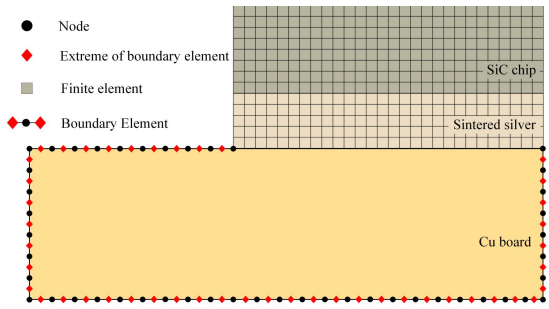

Fig. 5. Mesh diagram used by the FEM-BEM coupling algorithm.

Fig. 6 displays the stress distribution in sintered silver at t=0.05 s. For comparative purposes, the figure also includes

results obtained using the FEM, which employs a very fine mesh to enhance accuracy. From Fig. 6, it can be clearly seen that the coupling solution and the finite element solution are in good agreement overall.

(a) The stress distribution of the silver (Coupling algorithm)

(b) The Stress distribution of the silver (FEM)

Fig. 6. Stress distributions obtained by the coupling algorithm and FEM when t = 0.05 s.

In order to further verify the accuracy of the coupling method, the displacement results along the line L_1 (shown in Fig. 4) calculated by the coupling algorithm under different degrees of freedom are compared with those obtained by the finite element solution. From Fig. 7, it can be found that the displacement results obtained by the coupling algorithm are in good agreement with those obtained by the finite method.

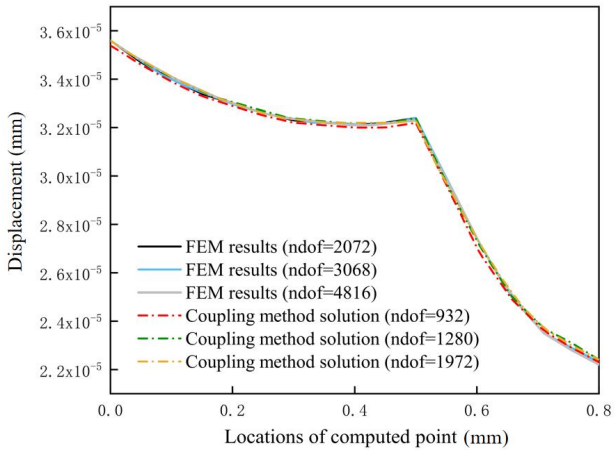

Fig. 7. The displacement obtained by different methods along the line L_1.

V. Conclusions

This paper proposed a FEM-BEM coupling algorithm to study the elastic dynamic response of electronic packaging structures. The model is divided into FE and BE domains based on the geometric characteristics or material properties of the model, which are solved using the FEM and the BEM respectively. Using the UEL subroutine in ABAQUS, the boundary element program is invoked to obtain the equivalent stiffness and load of the BE domain. These are then applied as predefined boundary conditions to solve for the unknown quantities in the FE domain. A numerical example is used to validate the accuracy and effectiveness of the results obtained by the coupling method in addressing transient elastic dynamic response problems in electronic packaging structures.

Acknowledgment

This research is supported by the National Natural Science Foundation of China (No. 12002009), R&D Program of Beijing Municipal Education Commission (No. KM202110005032).

References

[1] E. Suhir, M. Vujosevic, T. Reinikainen, “Nonlinear dynamic response of a ‘flexible-and-heavy’ printed circuit board (PCB) to an impact load applied to its support contour,” Journal of Physics D: Applied Physics, vol. 42, 045506, 2009.

[2] K. Sharan, S. Lahoti, J. Zhou, “Dynamic response of a portable electronic product subjected to an impact load,” Thermal and Thermomechanical Proceedings 10th Intersociety Conference on Phenomena in Electronics Systems, 2006. ITHERM 2006. IEEE, pp. 1049-1055, 2006.

[3] J. Xia, L. X. Cheng, G. Y. Li, B. Li, “Reliability study of package-on-package stacking assembly under vibration loading,” Microelectronics Reliability, vol. 78, pp. 285-293, 2017.

[4] M. A. Gharaibeh, J. M. Pitarresi, “An efficient equivalent static methodology for simulating electronic packages subjected to resonant vibrations,” Microelectronics Reliability, vol. 145, 115000, 2023.

[5] Y. V. N. Chandana, N. V. Kumar, “Drop test analysis of ball grid array package using finite element methods,” Materials Today: Proceedings, vol. 64, pp. 675-679, 2022.

[6] Z. Khatir, S. Lefebvre, “Boundary element analysis of thermal fatigue effects on high power IGBT modules,” Microelectronics Reliability, vol. 44, pp. 929-938, 2004.

[7] H. Yu, Y. Guo, Y. Gong, F. Qin, “Thermal analysis of electronic packaging structure using isogeometric boundary element method,” Engineering Analysis with Boundary Elements, vol. 128, pp. 195-202, 2021.

[8] G. Beer, I. Smith, C. Duenser, The boundary element method with programming: for engineers and scientists, Springer Science & Business Media, 2008.

[9] P. Zeng. Finite Element Analysis and Application, Tsinghua University Press, 2004

[10] H. M. Hilber, T. J. R. Hughes, R. L. Taylor, “Improved numerical dissipation for time integration algorithms in structural dynamics,” Earthquake Engineering & Structural Dynamics, vol. 5, pp. 283-292, 1977.

[11] J. Dominguez. Boundary elements in dynamics, Southampton and Boston: Computational Mechanics Publications, 1993.

[12] R. Song, F. Yuan, Y. Su, S. Wang, X. Zhang, “Infrared radiation-assisted non-pressure sintering of micron-sized silver for power electronic packaging,” Electronics, vol. 13, 1492, 2024.